High Temperature Corrosion of Materials (2024) 101:951–960
https://doi.org/10.1007/s11085-024-10282-7

ORIGINAL PAPER

Chlorine-Induced Stress Corrosion Cracking of Single Crystal Superalloys at 550 °C

F. Duarte Martinez[1] · Karl Dawson[2] · Gordon Tatlock[2] · J. Leggett[3] · G. Gibson[3] · J. C. Mason-Flucke[3] · J. R. Nicholls[1] · A. Syed[1] · N. Morar[4] · S. Gray[1]

Received: 15 July 2024 / Revised: 16 July 2024 / Accepted: 21 July 2024 /
Published online: 5 August 2024

Abstract

This study has investigated the effect of NaCl and different gaseous environments on the stress corrosion cracking susceptibility of CMSX-4 at 550 °C. The presence of SO_x leads to the rapid dissociation of NaCl into Na_2SO_4 and the release Cl_2 and HCl, which then trigger an active oxidation mechanism and stress corrosion cracking. The incubation time for crack initiation at 690 MPa and in the presence of a sulphur containing environment is 10 min. A working hypothesis is that stress corrosion cracking occurs due to the hydrogen released at the oxide/alloy interface when metal chlorides are formed; however, this hypothesis needs to be further explored.

Keywords Stress corrosion cracking · CMSX-4 · Hydrogen

Introduction

The synergistic effect of stress and deposit induced high temperature corrosion leads to the premature failure of aero turbine blades due to stress corrosion cracking. The lower shank of aero turbine blades, which operates below 600 °C is susceptible to this mode of failure. Two important factors that lead to stress corrosion cracking of single crystal nickel-based superalloys are the type of deposits that form on components (these include alkali chlorides and sulphates which are introduced through

✉ F. Duarte Martinez
Fabian.Duarte-martinez@cranfield.ac.uk

1 Department of Surface Engineering and Precision Institute, Cranfield University, Bedford MK43 0AL, UK

2 Department of Mechanical, Materials and Aerospace Engineering, University of Liverpool, Liverpool, UK

3 Rolls-Royce Plc, PO Box 31, Derby DE24 8BJ, UK

4 Department of Engineering, School of Science and Technology, University City of London, London, UK

the environment) and the concentration of SOx in the environment; typical sources of SOx are emissions from the oil and gas industry, power plants and volcanoes [1]. Therefore, it is important to understand the synergistic role of deposits and sulphur-containing gases on the stress corrosion cracking susceptibility of single crystal nickel-based superalloys below 600 °C.

Previous work has identified that $CaSO_4$ and Na_2SO_4 salts do not cause stress corrosion cracking in 400 h at 550 °C; however, chloride containing salts such as sea salt and NaCl can cause stress corrosion cracking in CMSX-4 at exposure times as low as 10 min at 550 °C but only in the presence of a sulphur-containing environment [2–4]. Nevertheless, a detailed investigation of the corrosion products that are formed with and without the presence of SO_x has not yet been explored. An understanding of this is crucial as the SO_x concentration in the atmosphere varies significantly in different regions of the world and has a seasonal dependence and this directly impacts the extent of attack on turbine blades.

The aim of this study is to investigate the effect of a 50 ppm SO_2_air atmosphere at 550 °C with no salt applied on CMSX-4, NaCl salt applied and exposed in air at 550 °C and NaCl salt in 50 ppm SO_2_air at 550 °C on the corrosion product and stress corrosion cracking susceptibility of CMSX-4. Investigation of these aspects has given a fundamental understanding of the corrosion mechanism, permitting a hypothesis regarding the mechanisms of embrittlement to be developed.

Experimental Procedures

CMSX-4 C-rings were provided by Rolls Royce plc. and were made with the < 001 > direction aligned with the cylinder axis (see Fig. 1). A maximum stress on the apex of the C-ring is applied by tightening the bolt, which in turn reduces the outer diameter of the C-ring. Finite element analysis was used to calculate the change in outer diameter required to achieve a target stress level, as described in Duarte et al. [3]. The secondary crystal orientation (SCO) was 36°. Although the SCO is not controlled during the manufacture of the C-rings, the displacement applied is calculated to achieve a target stress level for that specific SCO. At these SCO angles, the peak stress does not occur at the centre of the apex, it shifts towards the bottom washer (as shown in Fig. 1). The magnitude of the peak stress is 690 MPa in the middle region highlighted in Fig. 1d.

A jig developed by Rolls Royce Ltd (shown in Fig. 1a) was used as an automated tool to apply the desired displacement on the C-ring specimens. The C-ring is held in a jig, slotted into a nut holder which is spring loaded to keep the C-ring in place. A stepper motor tightens the bolt on the C-ring. The system measures the initial outer diameter of the C-ring, and subsequently the desired displacement is entered in the keypad. Both the stepper motor and laser are connected in a feedback loop through an Arduino, so the reduction in outer diameter is measured in situ as the bolt is tightened until it reaches the outer diameter of interest. The outer diameter measurement has an absolute uncertainty of 0.001 mm.

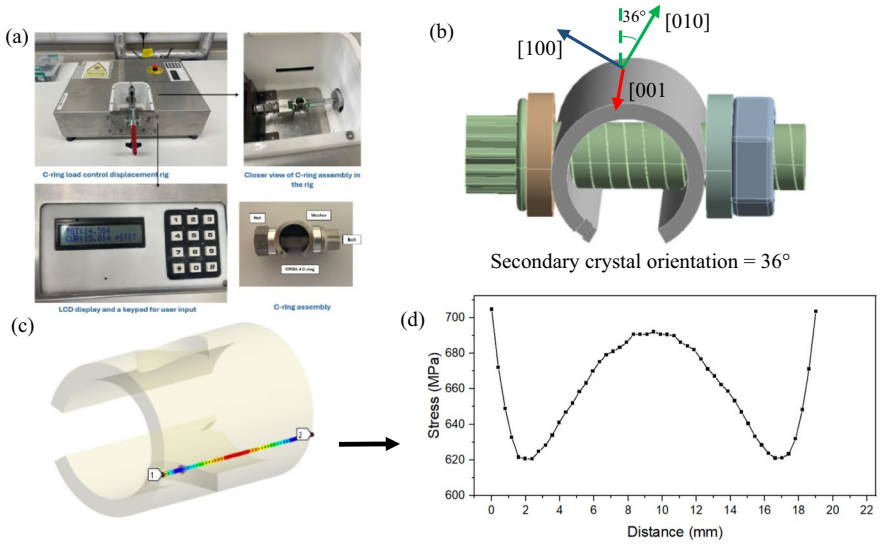

Fig. 1 **a** Jig used to apply stress on C-ring specimens, **b** secondary crystal orientation of C-ring, **c** stress distribution on C-ring specimen

Prior to salting, the specimens were cleaned using Isopropyl alcohol (IPA) and then placed on a hot plate at 200 °C. A saturated solution of deionised water + NaCl salt was used to spray the deposit onto the surface of the sample. Once the sample was heated, the saturated solution was sprayed onto its surface, which caused the water in the sprayed deposit to evaporate, leaving behind the salt. The salt flux used was 0.06 mg/cm^2 and an area of 3 cm^2 of the C-ring was salted, so a total of 0.18 mg salt was applied. This method enabled the formation of an adherent deposit on the surface.

A furnace with the capability of rapid heating was used for the low exposure times (1 min, 5 min, 10 min, 15 min). This furnace ramps up the temperature from 22–550 °C in approximately 3–4 min. Prior to these exposures, the SO_2 containing gas supply was left to stabilise for 15 min, and then the temperature was raised.

Focused ion beam (FIB) cross sections were done to study the microstructure of the scale formed below the salt deposits using a Tescan s8000. To perform the FIB cross sections a voltage of 30 keV and a beam current of 10nA. The backscattered electron images were done using a voltage of 20 keV and a beam current of 300 µA.

For the lamellae preparations, specimens were excavated from bulk samples by firstly depositing a layer of Pt, to protect the underlying material, before milling trenches either side of the region of interest. During the trenching and initial stages of milling an acceleration voltage of 30 kV and high beam current (21 nA) was used for fast material removal rates. The lamellae were released from the bulk sample, by making a J-cut incision and subsequently specimens were transported to Cu support grids, using the Omniprobe manipulator and attached to the grid with ion beam deposited platinum. A target thickness of approximately 80 nm was achieved by thinning with a 30 kV Ga ion beam and reduced beam currents (80 pA to 2.5 nA);

the lamellae were tilted ± 2° to the ion beam during this preparation step. Specimens were finished by applying a low kV (5 kV) polish to help remove material damaged by previous stages of thinning. Analytical TEM and STEM observations were performed using a LaB6 equipped JEOL 2100 + instrument, operating at 200kV. EDS analysis was carried out using an Oxford Instruments X-Max 65T EDS Detector and Aztec software.

Results

Figure 2 shows cross-sectional back-scattered electron images (the cross sections were produced by FIB) of a NaCl salted sample exposed in air and a NaCl salted sample exposed to 50 ppm SO_2_air that were previously reported by Duarte et al. [2]. The results of this study highlight that in the 400-h exposure, negligible internal attack (or less than 500 nm) was observed in the non-salted sample that was exposed to 50 ppm SO_2_air. However, on the NaCl salted sample exposed in air for 50 h (Fig. 2a), approximately 1µm of internal attack and corrosion products (mainly NiO and CoO) within the salt particle was observed. Similarly, for the NaCl salted sample exposed in 50 ppm SO_2 for 50 h (Fig. 2b), approximately 2 µm of internal attack and corrosion product (mainly Na_2SO_4, NiO and CoO) within the salt particle and an inner scale rich in Al, Cr, Ti, S, O and Cl was observed. The key observation is that no stress corrosion cracks were observed when no NaCl salt was applied and exposed to 50 ppm SO_2 in 400 h, and no cracks were observed when NaCl was applied, and the exposure was done in air only. Cracks initiated only when NaCl was exposed in the 50 ppm SO_2_air environment.

Sample Salted with NaCl and Exposed in 50 ppm SO_2_ Air at 550 °C

Figure 3 shows top surface secondary electron (SE) images of the first 10 min of exposure in a 50 ppm SO_2 environment. Within the first 5 min of exposure, a halo composed of Na_2SO_4 and NaCl surrounded the ridges and also shows dark spots rich

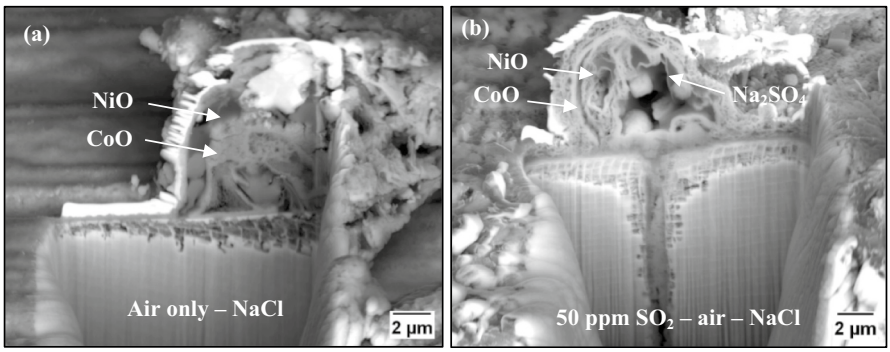

Fig. 2 Cross-sectional BSE images of **a** sample salted with NaCl and exposed to air and exposed to 50 h, **b** sample salted with NaCl and exposed to 50 ppm SO_2 and exposed to 50 h [2]

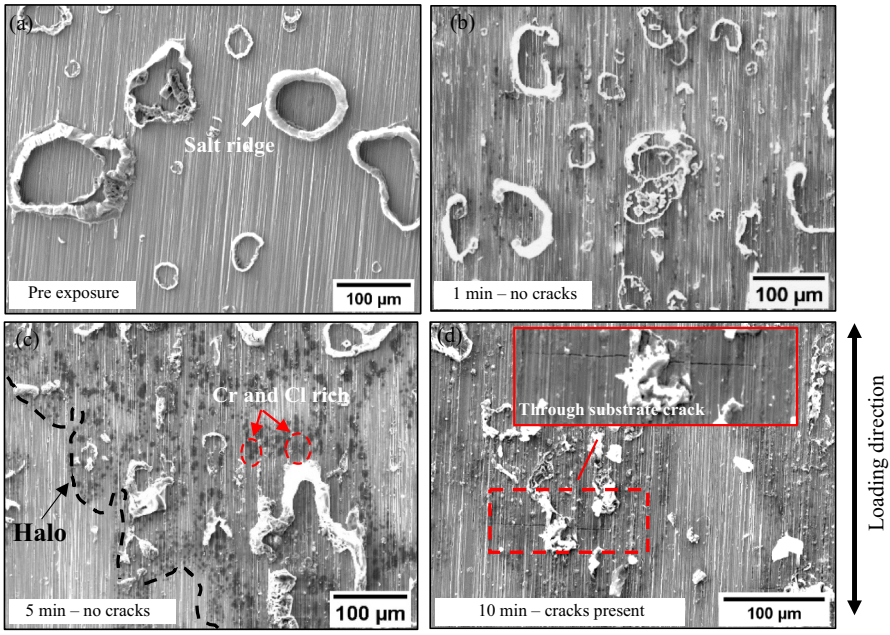

Fig. 3 Top surface SE images of C-ring salted with NaCl and exposed to 50 ppm SO_2 at 550 °C

in Cr and Cl appearing on the outline of the halo shown in Fig. 3c. The mechanism of the halo formation is not yet well understood but may have been produced due to the formation of a low melting point eutectic. In the early stages of the exposure, NaCl reacts with SO_x to form Na_2SO_4, but the eutectic temperature of Na_2SO_4_NaCl is 628 °C [5], which is above the test temperature, so it is not responsible for the formation of the halo. However, the HCl and Cl_2 that is released in the conversion of NaCl to Na_2SO_4 reacts with alloy elements to form $AlCl_3$, $TiCl_4$ and $CrCl_3$. These metal chlorides react with excess NaCl on the surface to form low melting point eutectics. For instance, the NaCl-$CrCl_2$ system has a melting point of 437 °C [6] and the NaCl-$AlCl_3$ has a melting point of 152 °C [7] and can form in the tested conditions. So, it is likely that the mechanism of halo formation involves an interaction of the metal chlorides with some excess NaCl on the surface. The halo spreads around the ridge of the salt, and after 10 min of exposure cracks initiate below the ridge, propagate and arrest at the boundary of the halo, as shown in the schematic of Fig. 4.

A lamella was produced from the 50 ppm SO_2_air exposed for 50-h sample to examine the corrosion products formed at the crack wake. The lamella was produced from a spalled region where a salt deposit was previously present. Based on the EDS analysis of Fig. 5a TiO_2 layer formed in the outer regions of the crack wake followed by a NiO and CoO layer. Inner Cr_2O_3, followed by a mix of Al_2O_3/$AlCl_3$ and internal sulphidation was observed. It is presumed that the sulphur was associated with tungsten forming WS_2 as identical structures have been observed in previous work [4]. Below the internal attack, the gamma channels seem to be depleted of alloy

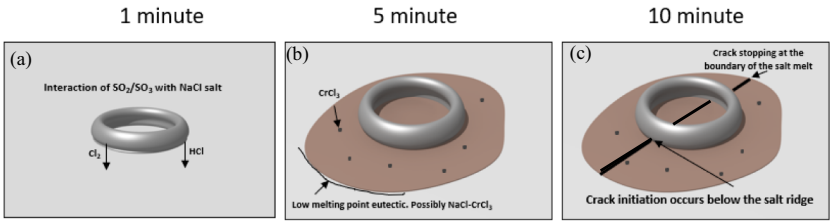

Fig. 4 Schematic showing the early stages of corrosion in a NaCl salted sample exposed to 50 ppm SO_2_air at 550 °C

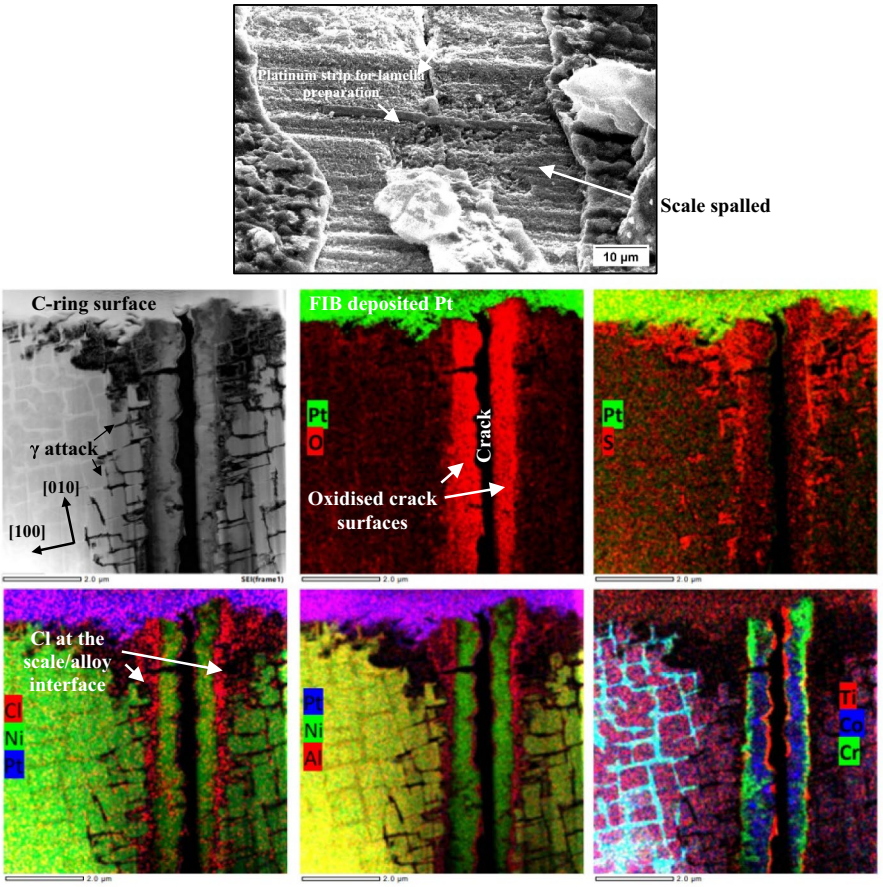

Fig. 5 TEM EDS map of C-ring exposed to 50 ppm SO_2_air at 550 °C for 50 h

elements, potentially due to the outward diffusion of Ni, Co, and Cr from the gamma matrix. Based on these observations, it is thought that the reaction of NaCl with SO_x to form Na_2SO_4 occurs in the very early stages, which releases Cl_2 and HCl,

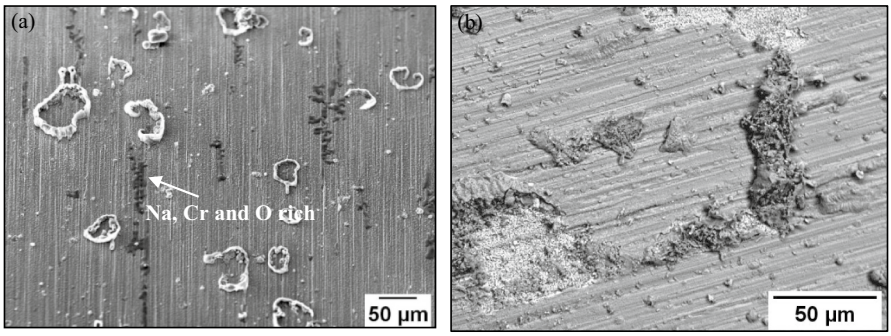

Fig. 6 Top surface images of C-ring salted with NaCl and exposed in air at 550 °C for 50 h

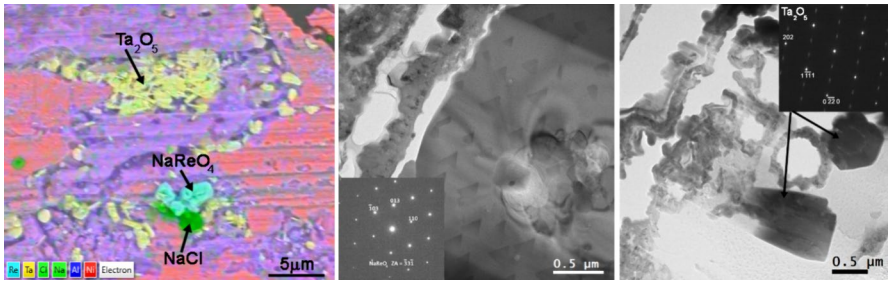

Fig. 7 **a** Underside of corrosion scale, **b** TEM/SAED identification of $NaReO_4$ and **c** Ta_2O_5

breakdowns the semi protective oxide and leads to a complex interplay of oxidation, chlorination and sulphidation.

Sample Salted with NaCl and Exposed in Air at 550 °C

The sample salted with NaCl and exposed in air at 550 °C did not show any stress corrosion cracks in 50 h of exposure and did not exhibit the halo that formed in the sample exposed in 50 ppm SO_2_air; however, some reactions of the oxide with NaCl were evident. For instance, Fig. 6a shows corrosion products rich in Na, Cr and O, potentially as $NaCr_2O_4$ and has been observed in previous work. The scale was loose, and scale spallation was observed where in regions where salt particles were present, as is shown in Fig. 6b. The loose scale enabled it to be torn off with tape to examine the underside of the scale. Particles rich in Na, Re and O were observed as well as Ta and O rich particles as observed in Fig. 7. A lamella was produced across one of the particles, and the electron diffraction pattern identified the phase to be $NaReO_4$, as shown in Fig. 7b. Similarly, electron diffraction identified Ta_2O_5 as shown in Fig. 7c. These interactions of NaCl with oxides enable the breakdown of the oxides and generate HCl and Cl_2. Some regions of the scale had unreacted NaCl, so it seems that the dissociation of NaCl does not occur as rapidly as in an SO_2 containing atmosphere.

Discussion

This study has shown that an atmosphere of air − 50 ppm SO_2 at 550 C without any salt applied causes negligible corrosion attack on CMSX-4 and no cracks form in a 400 h exposure time. When NaCl is applied, cracks form in the presence of a 50 ppm SO_2 environment in 10 min and no cracks are formed when the NaCl salted sample is exposed in air in 50 h. Undertaking the test in a sulphur containing atmosphere increases the alloy's susceptibility to stress corrosion cracking, and this susceptibility seems to be dependent on how rapidly NaCl can dissociate into corrosive Cl_2 and HCl.

The mechanism of NaCl dissociation depends on the test environment it is exposed in. On the one hand, the presence of SO_x leads to the dissociation of NaCl to Na_2SO_4 and the release of Cl_2 and HCl. This is highlighted in the phase stability diagram of Fig. 8 and Eq. 1, where Na_2SO_4 is the stable phase that forms at 1 atm O_2. Equation 1 assumes that H_2O is present in the test environment; however, a clear limitation of this study is that the concentration of H_2O has not been measured. Typically, low concentrations of H_2O are present as moisture in the test environment or as water crystallisation in the salt [8], but further work should concentrate in quantifying the amount of H_2O and investigate its effect on HCl formation. The kinetics of NaCl to Na_2SO_4 formation seems to be very rapid, as almost all the NaCl has converted to Na_2SO_4 after two hours. The release of HCl and Cl_2 lead to an active oxidation mechanism as proposed by Grabke [9], where volatile metal chlorides form, diffuse outward and oxidise causing the breakdown of the oxide. In conjunction to this, the breakdown of the oxide enables internal sulphidation to occur.

$$2NaCl(g) + SO_2(g) + 0.5O_2(g) + H_2O \rightarrow Na_2SO_4 + 2HCl\Delta G = -299202.0J \quad (1)$$

On the other hand, undertaking the exposure in air leads mainly to the vaporisation of NaCl, due to its high vapour pressure at 550 °C. Also, to some extent reactions of NaCl with Cr and Re to form mixed Na oxides have been observed. These

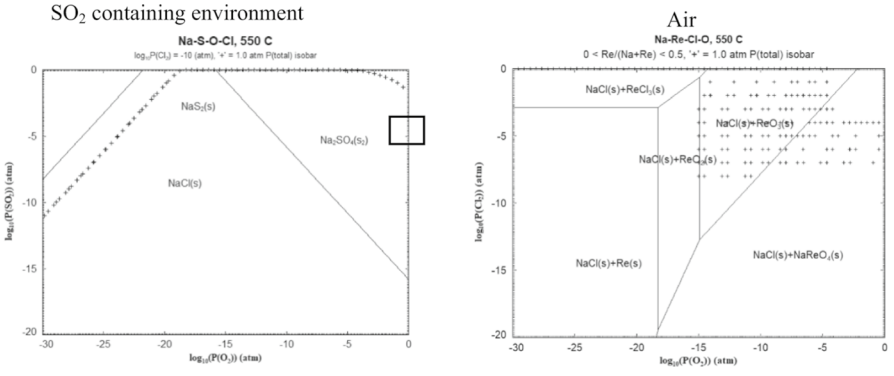

Fig. 8 Phase stability diagram of Na-Re–O at 550 °C

reactions release Cl_2 and HCl as shown in the equations below and, therefore, breakdown the protective oxide layer. However, the kinetics of this form of NaCl dissociation does not seem to be very rapid and no significant chlorination is observed.

$$NaCl(g) + 0.5Cr + 0.75O_2 + 0.5H_2O \rightarrow 0.5Na_2CrO_4 + HCl\Delta G = -292232.6J \quad (2)$$

$$NaCl(g) + Re + 0.5H_2O + 1.75O_2 \rightarrow NaReO_4 + HCl\Delta G = -526381.4J \quad (3)$$

The mechanism of embrittlement is not yet understood. The attack by sulphidation in the 50 ppm SO_2_air atmosphere may be important, as previous work has identified the significant embrittling effect of sulphur in nickel alloys by reducing the cohesion in grain boundaries [10]; however, its effect in single crystals has not yet been widely explored. In addition, previous work has highlighted that NaCl salt applied on Ti-alloys at temperatures up to 500 °C leads to the formation of Na_2TiO_3 and the release of HCl; they argue that the release of HCl is detrimental, as when it reacts with alloying elements it releases hydrogen to form Ti-hydrides and therefore embrittle the alloy [8]. Nevertheless, the effect of HCl on causing hydrogen embrittlement in single crystal nickel-based superalloys has not been investigated and needs further research.

Conclusions

This work highlights that the synergistic effect of a sulphur-containing environment and NaCl are critical in rapidly dissociating NaCl to form Na_2SO_4 and release Cl_2 and HCl to breakdown the oxide. The release of chlorine-containing gases leads to the formation of volatile metal chlorides, releasing hydrogen gas at the alloy/scale interface. Exposures in air lead to a different form of NaCl dissociation, as it reacts with Re and Cr to form Na-Re rich and Na-Cr rich oxides; however, stress corrosion cracking is not observed in 50 h of exposure when exposures are undertaken in air only. The mechanism of stress corrosion cracking needs further investigation; nevertheless, the formation of hydrogen at the alloy/scale interface when metal chlorides form or the attack by sulphur during sulphidation are important factors that need to be considered.

Acknowledgements We would like to thank Rolls Royce for funding and their invitation to take part in these studies. STEM and SEM experiments were performed in the Albert Crewe Centre and the SEM SRF, at the University of Liverpool, maintained and operated as a Shared Research Facility by the Faculty of Science and Engineering.

Author contributions Fabian Duarte Martinez wrote the manuscript, carried out the experimental work and lead the analysis of the results. Karl Dawson carried out the microscopy characterisation of the samples and supported in the discussion of the results. Gordon Tatlock carried out the microscopy characterisation of the samples and supported in the discussion of the results. Jonathan Leggett provided the samples and supported in the discussion of the results. Grant Gibson provided the samples and supported in the discussion of the results. Julian Mason Fucke provided the samples and supported in the discussion of the results. John Nicholls supported in the discussion of the results. Adnan Syed supported in the discussion of the results. Nicolau Morar supported in the discussion of the results. Simon Gray supported in the discussion of the results.

Data availability No datasets were generated or analysed during the current study.

Declarations

Conflict of interest The authors declare that they have no known competing financial interests or personal relationships that could have appeared to influence the work reported in this paper.

References

1. V. E. Fioletov, et al., *Atmospheric Chemistry and Physics* 16, 11497 (2016).
2. F. D. Martinez, et al., *Materials at High Temperatures* 40, 283 (2023).
3. F. D. Martinez *et al*., in *Superalloys* (2020), p. 753.
4. K. Dawson, et al., *Materials at High Temperatures* 40, 296 (2023).
5. Y. Niu, F. Gesmundo, F. Viani, and W. Wu, *Oxidation of Metals* 42, 265 (1994).
6. J. C. Shiloff, *The Journal of the Physical Chemistry* 64, 1566 (1960).
7. K. S. Mohandas, N. Sanil, T. Mathews, and P. Rodriguez, *Metallurgical and Materials Transactions B* 32, 669 (2001).
8. T. Chevrot, *Pressure Effects on the Hot-Salt Stress-Corrosion Cracking of Titanium Alloys*, (Cranfield University, 1994).
9. H. J. Grabke, E. Reese, and M. Spiegel, *Corrosion Science* 37, 1023 (1995).
10. J. P. Beckman and D. Woodford, in *Superalloys*1 (1988), p. 795.